Original Article

A Broadband Equivalent Model of On-Chip Spiral Inductors using Differential Evolution Algorithm

Vrinda. K[1], Dhanesh G. Kurup[2]

[1,2]*Department of Electronics and Communication Engineering, Amrita Vishwa Vidyapeetham, Bengaluru, India*

[1]k_vrinda@blr.amrita.edu, [2]dg_kurup@blr.amrita.edu

Abstract - *The article presents robust broadband lumped equivalent model for an on-chip spiral inductor which is an integral part of RF front end blocks. The frequency-independent model generation involves two steps- rational function modelling from two-port Scattering (S) parameters of the spiral inductor and a circuit extraction technique. The paper proposes a population-based Differential Evolution Algorithm for the rational function modelling of the inductor. Applying the Differential Evolution Algorithm ensures a more generalized and flexible model consisting of poles and residues. The nature of the poles and residues is determined by introducing a random floating-point vector, S_i, and is a unique contribution of this work. The proposed algorithm also eliminates the initial poles calculation step in the conventional modelling algorithms and makes the performance insensitive to the initial poles. Further, the paper illustrates an efficient circuit extraction methodology for generating a SPICE-compatible equivalent circuit from the identified poles and residues of the inductor. The equivalent model obtained in this work accurately predicts the initial increase and the eventual decrease in the series resistance due to skin/proximity effects and substrate coupling, respectively.*

Keywords — *Differential Evolution Algorithm, Circuit, Spiral inductor, Rational function model, Skin/ proximity effect.*

I. INTRODUCTION

The introduction of 5G and the Internet of Things (IoT) communication platforms have driven increasing global demand for faster and smaller consumer devices and systems [1],[2]. On the other hand, the significant technology innovations in the chip industry have also helped cater to the customer needs for smaller low-power devices. The scaling down of the device dimension into deep sub-micron levels allowed the integration of complex high-frequency circuits along with the analog and digital baseband circuits on the same wafer [3]. This heterogeneous integration facilitates the integration of more passive devices such as transmission lines,

vias and spiral inductors onto the wafer [4],[5]. All these factors make the system-level design of the present-day RFICs highly complex, warranting the design with high-frequency electromagnetic interference between linear and non-linear devices [6],[7]. Therefore, accurate modelling and prediction of such electromagnetic effects are critical

for accurate system-level static-timing and signal integrity analysis [8],[9]. However, the electromagnetic effects are primarily dependent on the physical and material properties of the device under consideration. They, therefore, can only be analyzed and studied on Electromagnetic Field Solvers such as HFSS [10]. On the other hand, a system-level performance analysis of an RFIC is done using time-domain simulators such as CADENCE Spectre RF for accurate transient simulations [11]. Therefore, it is necessary to model and characterize the passive RF devices and their electromagnetic effects efficiently such that the resulting model can be easily integrated into a time-domain simulation environment for accurate transient simulations. A design that ignores the efficient passive device modelling fails at the sign-off phase because of the signal integrity violations [12].

The most challenging passive device modelling is the spiral inductor modelling because of its intrinsic geometry and the device's area on the silicon wafer. Many significant electromagnetic effects can limit the performance of the spiral inductor, such as proximity effect, skin effect, dielectric coupling, and substrate coupling [13]. It is studied that the spiral inductor's series resistance (R_s) initially increases due to proximity and skin effects and further decreases pertaining to the silicon substrate coupling [14]. Although many previous pieces of literature present different spiral inductor models, most fail to model these characteristics of R_s over a wide frequency band. For instance, [15] presents a classical empirical closed-form model of the spiral inductors. Nevertheless, the model does not contribute much towards predicting the complex frequency-dependent effects. Besides, closed-form models involve tedious and time-consuming analysis, which increases the design cycle duration and time to market the final products. Moreover, empirical models depend on the device's physical characteristics and operation frequency and therefore become difficult to incorporate in a time-domain simulation environment [16],[17]. On the other hand, many researchers have reported frequency-independent models of inductors [18]-[20]. In [18], and augmented approach of modelling the spiral inductor incorporating the compact circuit modelling and broadband modelling is adopted. The methodology is clever. However, the scenario in [18] does not consider the substrate coupling effects. Similarly, in [19], a scalable broadband model captures the proximity and skin effects,

but the equivalent circuit requires a chain of ladder networks and becomes complex for the higher order of approximations. Further, [20] presents accurate modelling for substrate coupling in on-chip spiral inductors. However, the model in [20] is an analytical model, and therefore, the approach becomes tedious and time-consuming. One of the recent works in [21] presents a scalable broadband spiral inductor model with considerable accuracy. It is understood that the model characterizes the series resistance as a linear function of frequency and fails to capture the decrease in series resistance due to silicon substrate coupling. Based on the literature survey, one of the most straightforward modelling approaches is broadband modelling, where the frequency response is approximated to a compact mathematical form. Further, [22] presents a rational function-based broadband inductor model with frequency-independent elements. The least-square approximation-based rational function technique used in [22] approximates the input-output frequency response of the device into a pole-residue form. Although a broadband modelling methodology is implemented in [22], the substrate coupling effect is not modelled in this work. In addition to this, the accuracy of the existing rational function modelling technique is sensitive to the selection of initial poles [23],[24]. An equivalent circuit model is presented in [25] that accurately predicts non-linear series resistance characteristics over a broad frequency range. However, the model generation is based on extended synthesis and analysis steps, and the extracted model is complex with a greater number of circuit elements.

This article presents a broadband π equivalent lumped model that accurately models the spiral inductor's series resistance, series inductance, and quality factor. The circuit element values used in this model are extracted from a set of poles and residues identified using a population-based optimization algorithm called Differential Evolution Algorithm (DEA) [26],[27]. Unlike the existing rational function methodologies, DEA is more flexible because the algorithm does not require the initial pole calculation step and has the inherent ability to handle non-uniform and noisy input data. The methodology represents the candidate solutions as floating-point numbers and takes the vector differences of the floating-point candidate solutions to achieve the optimization criteria [28]. The previous literature suggests that DEA is not much applied to passive RF devices' rational function modelling except for [29]. According to the literature survey, no previous literature reports the application of DEA for broadband modelling of on-chip spiral inductor from the device input-output frequency response characterized by two-port scattering parameters. Given the frequency response, DEA finds the optimal set of poles and residues by minimizing an error function into a global minimum value. Once DEA identifies the pole-residue parameters, the corresponding circuit component values are synthesized using an efficient circuit extraction methodology [30]. To validate the proposed model accuracy, the series resistance, inductance and quality factor of the model is compared with the

measured response of the spiral inductor fabricated in [25]. The proposed equivalent model is proven to accurately model the series resistance decrease and the series inductance and quality factor characteristics. The detailed methodology of rational function modelling using DEA is illustrated in the next section. The methodology to extract the values of R, L, C components from the identified pole-residue model is also illustrated. The results section provides the simulation results for the modelling and analysis of the fabricated spiral inductor in [25] using DEA.

II. METHODOLOGY FOR THE MODEL EXTRACTION OF ON-CHIP SPIRAL INDUCTOR

A. Rational Function Modeling Using Differential Evolution Algorithm

DEA is an evolutionary optimization algorithm that optimizes a problem by iteratively improving the candidate solution with respect to certain constraints assumed according to the problem criteria. Therefore, given the frequency domain input-output response of the on-chip spiral inductor, defined by $f(s)$ over a finite frequency range, DEA approximates into a partial fraction form, $f_m(s)$, consisting of poles and residues as in the expression follows,

$$f(s) \approx \frac{N(s)}{D(s)} = \sum_{k=1}^{K} \frac{C_k}{s - A_k} = f_m(s) \qquad (1)$$

where C_k and A_k Are the residues and poles of the system, and K is the order of approximation, respectively. $f_m(s)$ represents the model and s = j ω represents *the nth* frequency of N point discrete frequency domain data. The goal of the methodology is to determine the accurate set of the optimal parameters, C_k and A_k , $k = [1:K]$ of the rational function model, which approximates the given frequency domain response, $f(s)$ according to the criteria formulated as follows,

$$\sum_{n=0}^{N-1} |f(s_n) - f_m(s_n)|^2 \qquad (2)$$

We know that the optimal parameters comprising poles and residues of the rational function model, $f_m(s)$ It can be complex or real. Therefore, the poles and residues can be expressed as,

$$C_k = \alpha_k + j\beta_k \qquad (3a)$$

$$A_k = \gamma_k + j\eta_k \qquad (3b)$$

where α_k , β_k and γ_k , η_k corresponds to the real and imaginary parts of the residues and poles, C_k and A_k , respectively. The nature and domain of optimal parameters are critical to model the transfer function since poles and residues determine the physical realizability of the model. For any system to be realizable, the input-output port system transfer function encapsulating the system behaviour must be a positive-real function. The real positive nature of the transfer function thus imposes the following constraints on the nature of the poles and residues of the model,

$$if \quad \beta_k = 0, \eta_k = 0 \qquad (4)$$

On the contrary,

$$C_k^* = \alpha_k - j\beta_k \qquad (5)$$

$$A_k^* = \gamma_k - j\eta_k \qquad (6)$$

(4), (5) and (6) imply that if the pole is real, the corresponding residue must be real. On the other hand, if a pole is complex, the corresponding residue also must be complex. In that case, a complex conjugate of the respective pole and residue always exists such that the resulting transfer function is positive-real. The criteria in (5) and (6) conclude that if a pole or residue is complex, the corresponding conjugates are obvious. Therefore, the algorithm need not have to find the conjugates. This approach enables us to reduce the algorithm's computational complexity by solving for fewer parameters. Another factor to be considered is the criterion imposed on the location of the system poles, represented as follows,

$$\gamma_k < 0 \qquad (7)$$

The criteria mentioned in (7) states that all the poles of a realizable system should always lie on the left half side of the complex S-plane to comply with the BIBO (Bounded Input Bounded Output) stability criterion. The above criteria imposed on the domain and nature of the optimal parameters necessitates the model in (1) to be conditioned and reformulated as follows,

$$f_m(s) = \sum_{k=1}^{K} \frac{\alpha_k + jS_k\beta_k}{s - (\gamma_k + jS_k\eta_k)} + \frac{\alpha_k - jS_k\beta_k}{s - (\gamma_k - jS_k\eta_k)} \qquad (8)$$

where S is a random floating-point vector incorporated in the algorithm to determine the nature of the poles and residues of the model in (8). S_k takes the values 0 or 1 to impose the following criteria on the model,

$$C_k, C_k^* = \alpha_k \pm j\beta_k, if \ S_k = 1 \qquad (9a)$$

$$C_k = \alpha_k, \ if \ S_k = 0 \qquad (9b)$$

Similarly,

$$A_k, A_k^* = \gamma_k \pm j\eta_k, if \ S_k = 1 \qquad (10a)$$

$$A_k = \gamma_k \ if \ S_k = 0 \qquad (10b)$$

(9a) and (10a) implies that if $S_k = 1$, corresponding poles and residues are assumed in complex conjugate pairs. Else if, $S_k = 0$, corresponding poles and residues are assumed to be real. Therefore, rational function modelling of on-chip spiral inductors using DEA consists of finding the optimal parameters of the model in (8) such that $f_m(s)$ best approximates the given frequency domain response, $f(s)$ Which can be formulated as an optimization problem that aims to reduce a frequency domain error function as given in (2).
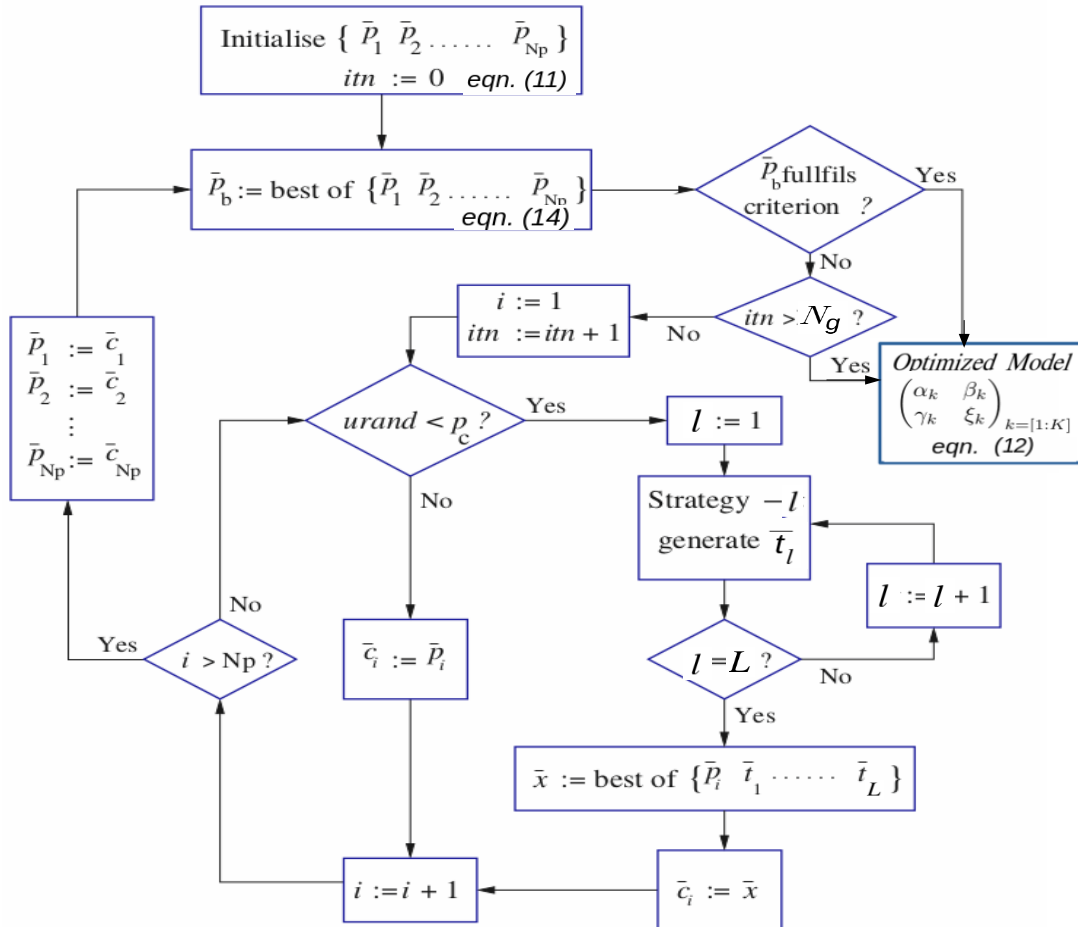
Fig.1 The Framework of Differential Evolution Algorithm for Rational Function Approximation.

The flowchart illustrated in Fig. 1 gives the complete framework of the proposed DEA for the rational function modelling of passive RF devices [28]. Therefore, given the frequency domain response of a device characterized by the scattering parameters, DEA creates an initial parent population of size, N_p, uniformly distributed over the parameter space for the first iteration, $itn = 0$, as follows,

$$\overline{P}^{(0)} = \begin{bmatrix} \overline{p}_1 & \overline{p}_2 & \cdots & \overline{p}_{N_p} \end{bmatrix} \tag{11}$$

where $\overline{p}_i$, i=[1:N$_p$] represents D dimensional floating-point vectors consisting of the model parameters to be computed by DEA given by,

$$\overline{p}_i = [\alpha_1 \; \alpha_2 \; \alpha_3 \; \ldots \; \alpha_K \; \beta_1 \; \beta_2 \; \beta_3 \; \ldots \; \beta_K$$
$$\gamma_1 \; \gamma_2 \; \gamma_3 \; \ldots \; \gamma_K \; \eta_1 \; \eta_2 \; \eta_3 \; \ldots \; \eta_K \; S_1 \; S_2 \; S_3 \; \ldots \; S_K] \tag{12}$$

Hence, the total number of parameters to be optimized, D is given by,

$$D = 5K \tag{13}$$

Once the initial parent population is created, DEA finds the best parent population, $\overline{P}_b$, represented as given below,

$$\overline{P}_b = best \; of \begin{bmatrix} \overline{p}_1 & \overline{p}_2 & \cdots & \overline{p}_{N_p} \end{bmatrix} \tag{14}$$

If the best parent population, $\overline{P}_b$ meets the optimization criterion, or if the number of iterations, itn, reaches the maximum specified number of iterations or generations, N$_g$, the algorithm terminates. Therefore, the best parent population members become the optimal model parameters (12). Else, members in the parent population, $\overline{P}^{(0)}$ Are iteratively refined and replaced by the new set of members using two operations, namely, mutation and cross-over. The algorithm generates a new set of vectors called trial vectors, l, for every p_i That can replace the parent members in the initial parent population. The trial vectors, t_l, $l = [1:L]$ are generated using L different strategies as discussed in [28]. The trial vectors generated are checked for the boundary conditions mentioned (4), (5) and (6). If any member in trial vectors is out of search space, the corresponding member is updated such that the member is within the search space marked by the constraints defined. For every iteration and a given member, either the newly generated trial members become the child, or the algorithm retains the members in the parent population to become the child. This decision depends upon a probability parameter that uses a random number generator, urand. The random number generator is implemented to generate random numbers that are uniformly distributed in the range [0,1], such that the probability of the child becoming a parent is p_c and the probability of trial members becoming the child is 1-p_c. Further, the algorithm computes the objective or cost function value for each child member. For an iteration, if the objective function value calculated for each child member is less than the corresponding value for a parent member, the parent will be replaced by the child member. This process generates a new parent population consisting of a set of potential parameters for the next iteration [28]. Therefore, the new members consisting of poles and residues obtained either from child or parent are refined over iterations until the optimal parameters are obtained.

B. Circuit Extraction Methodology

Once the optimal parameters are found, the lumped R, L, C component values can be extracted using an efficient circuit extraction technique. This work aims to model the spiral inductor into an equivalent π circuit, as shown in Fig. 2.
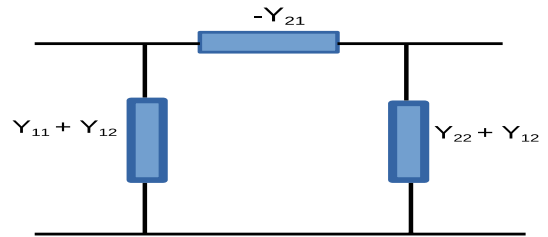
Fig.2 Equivalent π circuit obtained from the Admittance (Y) parameters.

The circuit in Fig. 2 is synthesized in terms of the frequency domain Admittance (Y) parameters that are closely related to the spiral inductor parameters as follows,

$$S_{21} = -Y_{21} \tag{15}$$

$$R_s + j\omega L_s = -\frac{1}{Y_{21}} \tag{16}$$

$$Q = -\frac{\text{Imag}(Y_{11})}{\text{real}(Y_{11})} \tag{17}$$

In order to synthesize the equivalent lumped circuit, first, the two-port Y parameters are approximated into the pole-zero form using DEA. Secondly, according to the following extraction steps, the identified poles and residues translate into the lumped RLC combination as shown in Fig. 3(a) and Fig. 3(b).

$$L_l = \frac{1}{C_l} \tag{18}$$

$$R_l = -L_l \; A_l \tag{19}$$

where L and R are the inductance and resistance values corresponding to the real poles and residues identified using DEA and translates to the circuit combination in Fig. 3(a). The number of RL circuits equals the number of identified real poles. Similarly, if the identified poles and residues are complex pairs, they translate to the circuit in Fig. 3(b), whose lumped component values are as follows,

$$L_{1m} = \frac{1}{C_k + C_{k+1}} \tag{20}$$

$$R_{1m} = \frac{-(A_k + A_{k+1}) + (C_k A_{k+1} + C_{k+1} A_k)}{C_k + C_{k+1}} \quad (21)$$

$$C_{1m} = \frac{C_k + C_{k+1}}{(A_k + A_{k+1}) + R_{1m} L_{1m}} \cdot \frac{C_k + C_{k+1}}{C_k A_{k+1} + C_{k+1} A_k} \quad (22)$$
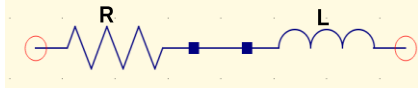
Fig. 3(a). Equivalent circuit synthesized from real pole/residue.
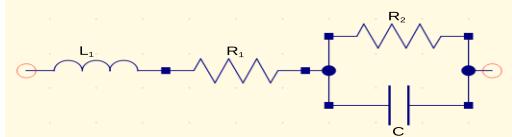
Fig. 3(b). Equivalent circuit synthesized from complex pole- residue pair.

III. RESULTS

To illustrate and validate the accuracy of the methodology and the model, a rectangular spiral inductor fabricated using 0.18 μm CMOS process, as discussed in [25], is used. Fig. 4 shows the layout of a 2.5 turn on-chip spiral inductor with the following dimensions, W×R×S (μm) =14.5×60×2.
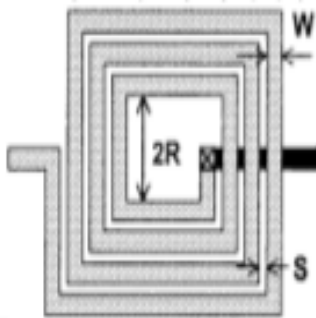
Fig. 4 On-chip spiral inductor layout.

In this work, since the goal is to synthesize a circuit model corresponding to Y parameters, the measured S parameters of the spiral inductor are converted into Y parameters. The Y parameters are given as the input to the Differential Evolution Algorithm with the population size, N_p =300, and the number of generations, N_g =10000. The nature and the order of the poles and residues must be found using DEA. It is observed that DEA approximates the $Y_{11} + Y_{12}$ and $Y_{21} + Y_{22}$ parameters at ports 1 and 2 of Fig. 2 accurately into a rational function with the order of approximation, K=6. The estimated Root Mean Squared Error (RMSE) of the model is 6.23×10^{-8}. Similarly, DEA approximates the $-Y_{21}$ with an order of approximation, K= 5 and RMSE = 1.05×10^{-5}. Fig. 5(a) and Fig. 5(b) show the DEA's performance in modelling the spiral inductor's Y parameters. It can be observed that DEA models the spiral inductor's two-port Y parameters

accurately, and the modelled response shows remarkable agreement with the actual response. The optimal parameters obtained using DEA, consisting of identified poles and residues, are tabulated in Table. I. Table. I show that DEA approximates $Y_{11} + Y_{12}$ with the order of approximation, K=6 consisting of two complex conjugate pairs and two real pole-residues sets. Similarly, DEA approximates Y_{21} with K=5, comprising one complex conjugate pair and three real pole-residue sets.

Further, the spiral inductor's physical parameters such as series resistance (R_s), inductance (L_s) and the quality factor (Q) are extracted from the modelled Y parameter, according to (15), (16) and (17). The results showing the comparison between the actual and modelled physical parameters of the spiral inductor are given in Fig. 6(a), Fig. 6(b), and Fig. 6(c), respectively.
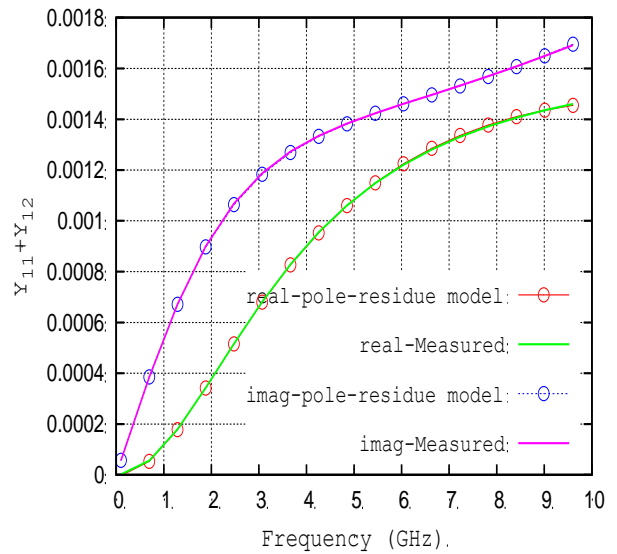
Fig. 5(a) Comparison between the actual and modelled response of the two-port Y parameter, Y₁₁+Y₁₂ using
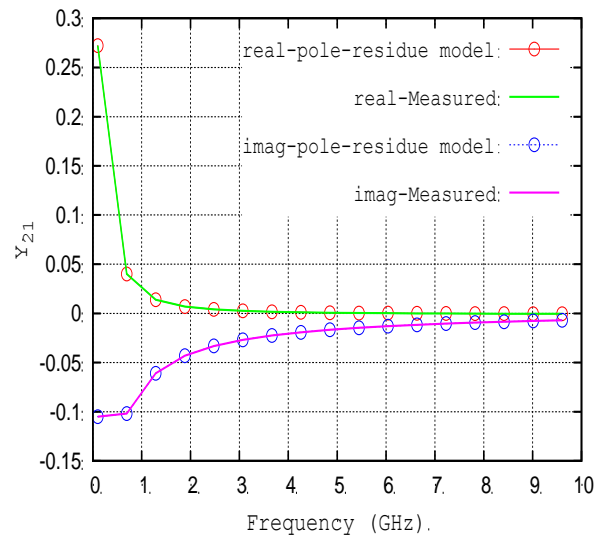
Fig. 5(b) Comparison between the actual and modelled response of the two-port Y parameter, Y₂₁ using DEA.

Table. I. Poles and Residues of the Y parameter rational function model of 2.5 Turn Spiral Inductor using Differential Evolution Algorithm.

Y parameter	Poles identified	Residues identified
$Y_{11}+Y_{12}$	$-4.03e^{11}$ $\pm 8.077e^{9}i$	$-4.03e^{7}$ $\pm 9.53e^{9}i$
	$-6.45e^{11}$ $\pm 7.10e^{12}i$	$4.33e^{11}$ $\pm 2.17e^{10}i$
	$-1.753e^{12}$	$-3.7980e^{9}$
Y_{21}	$-2.3507e^{9}$	$-3.989e^{7}$
	$-9.993e^{12}$	$2.286e^{11}$
	$-1.6126e^{9}$	$4.9978e^{8}$
	$-1.1928e^{10}$	$4.612e^{7}$
	$-2.840e^{11}$ $\pm 1.418e^{9}i$	$-5.313e^{9}$ $\pm 3.948e^{11}i$

The results in Fig. 6(a), Fig. 6(b) and Fig. 6(c) illustrate that the rational function model generated using DEA can model the series resistance, inductance and the quality factor, respectively accurately. The graph in Fig. 6(a) shows the accurate modelling of R_s that increases initially due to proximity and skin effects and eventually decreases pertaining to the silicon substrate coupling.
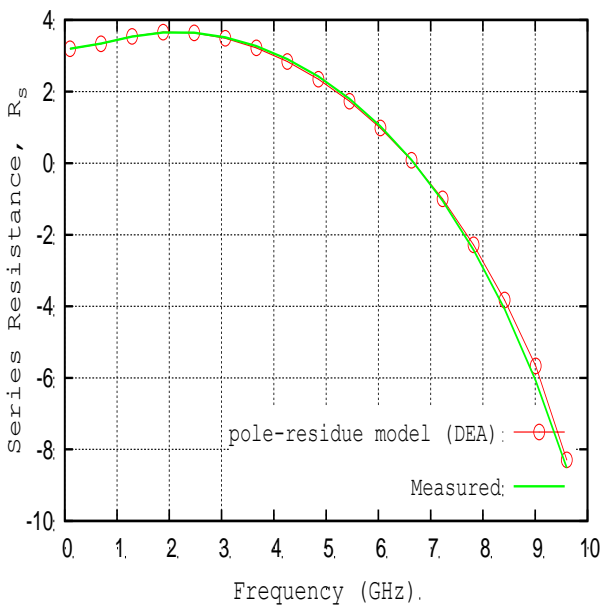
Fig. 6(a) Series Resistance modelling (R_s) using DEA and comparison with the actual series resistance of the spiral inductor.
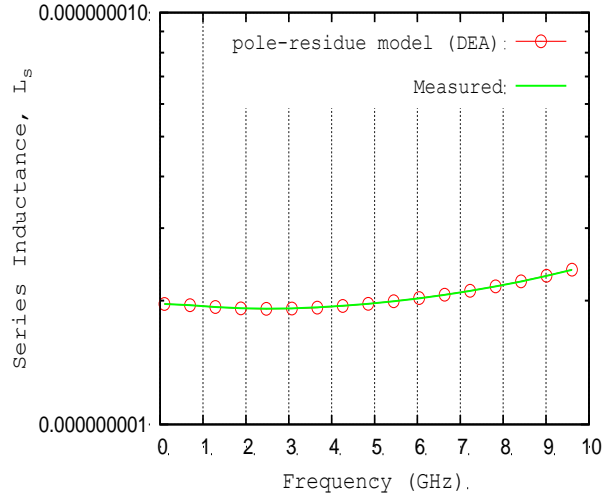
Fig. 6(b) Series inductance (L_s) modelling using DEA and Comparison with the actual series inductance of the spiral inductor.
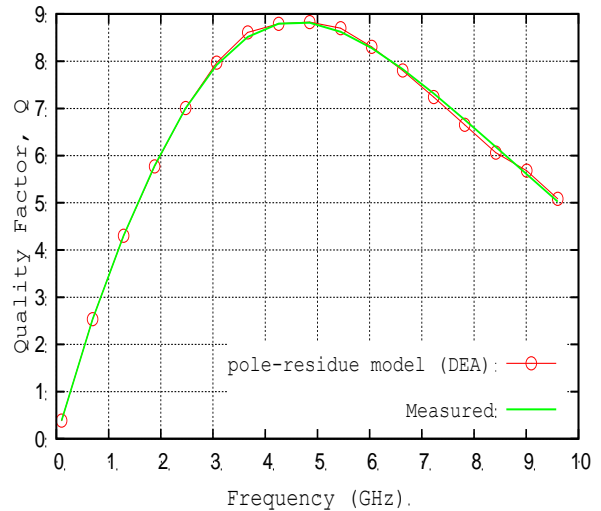
Fig. 6(c) Quality Factor (Q) modelling using DEA and comparison with the actual series inductance of the spiral inductor.

Further, the identified poles and residues are tabulated in Table. I are converted into an equivalent circuit in Fig. 2 using the circuit extraction methodology explained in section. II-B. The extracted lumped component values are tabulated in Table. II.

The accuracy of the extracted lumped equivalent model is validated by performing a scattering parameter simulation of the circuit in a time-domain circuit simulator like QUCS. Fig. 7(a) and Fig. 7(b) show the comparison between the spiral inductor's measured two-port S parameters and the synthesized circuit model response. It can be concluded that the model response is highly accurate since it shows clear agreement with the measured spiral inductor response.

Table. II. RLC values were extracted from the identified pole-residue rational function model obtained using DEA.

Y parameter	R	L	R_1	L	R_2	C
$Y_{11}+Y_{12}$	461.46	$2.63e^-$	732.88	$1.23e^{-9}$	$1.93e^1$	$2.37\ldots$
	589.19	$2.50e^-$	1.15	$1.15e^{-1}$	$5.84e^1$	$5.91\ldots$
	258.59	$2.16e^-$	36.64	$9.41e^{-1}$	$7.12e^1$	$7.37\ldots$
Y_{21}	3.226	$2.08e^-$				
	43.726	$4.37e^-$				
	461.46	$2.63e^-$				
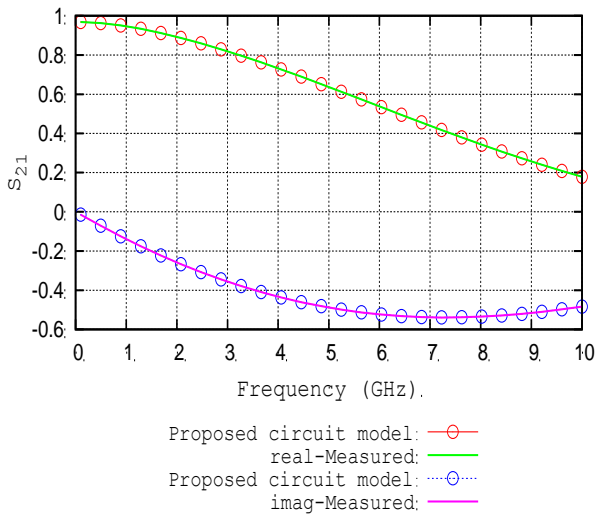
Fig. 7(a) Comparison between the actual and modelled S_{21} response of the spiral inductor.
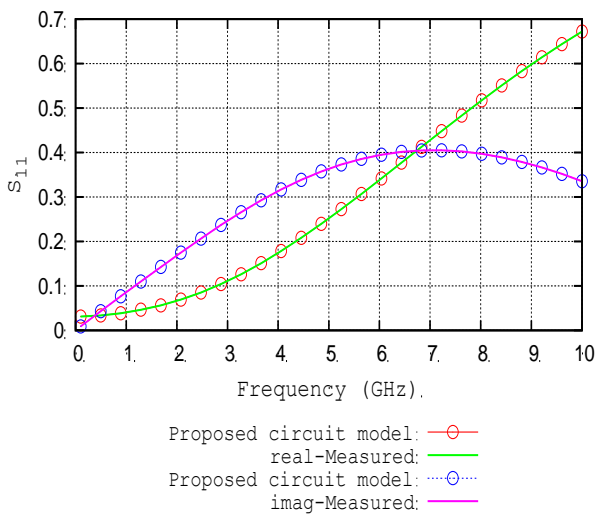
Fig. 7(b) Comparison between the actual and modelled S_{11} response of the spiral inductor.

From the studies, it is clear that the methodology and the equivalent circuit model illustrated in this paper are highly accurate and capable of modelling the skin effects, proximity effects and substrate coupling in on-chip spiral inductors. It is also found that the equivalent circuit model in this work needs fewer components than the existing spiral inductor models.

IV. CONCLUSION

A broadband SPICE compatible equivalent model for the on-chip spiral inductor is presented in the article. First, a rational function model consisting of poles and residues is obtained using an efficient population-based evolutionary algorithm, namely, Differential Evolution Algorithm. The results show that DEA identifies the accurate set of poles and residues using floating-point vector, S_k. Further, the identified poles and residues are translated into equivalent lumped RLC circuits using a circuit extraction methodology. The circuit model generated is highly accurate and is capable of predicting the series resistance (R_s), inductance (L_s) and quality factor (Q) accurately. The spiral inductor model in this article accurately models the decrease in series resistance due to substrate coupling, which is a significant parameter that most existing models fail to capture. We have also seen that the equivalent model requires a minimum number of circuit components and is efficient for time-domain simulations.

REFERENCES

[1] Kanti Prasad, Abdul Syed, RF-Microwave Double-Balanced Diode Mixers as Up-Converter MMIC module in RF Front End Transmitter Section for 5G Communications, International Journal of Electronics and Communication Engineering. 8(7) (2021) 1-10.

[2] Nitesh Gaikwad, Shiyamala. S. Design and Development of Microarchitecture for Dynamic IoT Communication, International Journal of Engineering Trends and Technology (IJETT). 69(11) (2021) 1-8.

[3] R. Achar, Modeling of High-Speed Interconnects for Signal Integrity, IEEE Microwave Magazine. 7(1) (2008) 61-74.

[4] S. Lefteriu and Stefano Grivet-Talocia, Topological Fitting: broadband modelling of passive components via augmented equivalent circuit model, IFAC-Papers Online, Elsevier. 51(2) (2018) 451-56.

[5] Praggya Agnihotry, R. P. Agarwal, Graphene-Based Planar VLSI Interconnects, International Journal of Engineering Trends and Technology (IJETT). 22(6) (2015)253-254.

[6] J. L. Herring, P. Naylor and C. Hristopoulos, Transmission-line Interconnect Models, IEEE Transactions on Advanced Packaging. 30(7) (2007) 795-807.

[7] Akshay Kumar, Amarveer Singh, Ekambir Sidhu, Equivalent Circuit Modelling of Microstrip Patch Antenna (MPA) Using Parallel LCR Circuits, International Journal of Engineering Trends and Technology (IJETT). 25(4) (2015) 183-185.

[8] S. G. Talocia and R. Trinchero, Behavioral, Parameterized, and Broadband Modeling of Wired Interconnect with Internal Discontinuities, IEEE Transactions on Electromagnetic Compatibility, 60(1) (2017) 77-85.

[9] J. E. Schutt-Aine et al., Comparative Study of Convolution and Order Reduction Techniques for Blackbox Macro modelling Using Scattering Parameters, IEEE Transactions on Components, Packaging and Manufacturing Technology. 1(10) (2001) 1642-50.

[10] Ansoft, User's Guide-High Frequency Structure Simulation Reference Manual. (2005).

[11] Cadence Design Systems, PSPICE User's guide. Second Edition. (2000).

[12] Sharad Kapur and David. E. Long, Modeling of integrated RF

passive devices, IEEE Custom Integrated Circuit Conference. (2010) 1-8.

[13] M. Dhamodaran et al., On-Chip Spiral Inductors and On-Chip Spiral Transistors for Accurate Numerical Modeling, Journal of Magnetics. 23(1) (2018) 50-54.

[14] Niranjan A. Talwalkar et al., Analysis and Synthesis of On-Chip Spiral Inductors, IEEE Transactions on Electron Devices. 52(2) (2005) 176-182.

[15] S. S. Mohan et al., Simple, accurate expressions for planar spiral inductances, IEEE Journal of Solid-State Circuits. 34(10) (1999) 1419-24.

[16] A. M. Niknejad, R. Gharpurey, and R. G. Meyer, Numerically stable Greens Function for modelling and analysis of substrate coupling in integrated circuits, IEEE Transactions on Computer-Aided Design Integrated Circuits Systems. 17(4) (1998) 305-15.

[17] F. W. Grover, Inductance Calculations: Working Formulas and Tables, Courier Corporation. (2004).

[18] Bo Han et al., Pole-zero analysis and broadband equivalent circuit for on-chip spiral inductors, International Journal of Numericals Modelling: Electronic Networks, Devices and Fields. 30(7) (2007) 795-807.

[19] X. Huo et al., A physical model for on-chip spiral inductors with accurate substrate modelling, IEEE Transactions on Election Devices. 53(12) (2006) 2942-49.

[20] H. Wang et al., Transfer Function Analysis and Broadband Scalable Model for On-Chip Spiral Inductors, IEEE Transactions on Microwave Theory and Techniques. 51(7) (2011) 1696-1708.

[21] Sathya Sree Jayaraman et al., A Scalable, Broadband, and Physics-Based Model for On-Chip Rectangular Spiral Inductors, IEEE Transactions on Magnetics. 55(9) (2019) 1-7.

[22] Y. Liang, Y. Wang. Lei Li, Rational modelling of the on-chip inductor by vector fitting, Analog Integrated Circuit and Signal Processing. 65(12) (2015) 253-58.

[23] B. Gustaven and A. Semlyen, Rational Approximation of Frequency Domain Responses by Vector Fitting, IEEE Transactions on Power Delivery. 14 (3) (1999) 1052-61.

[24] Vrinda. K and D. G. Kurup, Performance of Vector Fitting Algorithm Applied to Bandpass and Baseband Systems, Circuits, Systems and Signal Processing, Springer. 37(11) (2018) 5143-60.

[25] J. Gil and H. Shin, A Simple Wide-Band On-Chip Inductor Model for Silicon-Based RF ICs, IEEE Transactions on Microwave Theory and Techniques. 51(9) (2003) 2023-28.

[26] R. Storn, System design by constrained adaptation and differential evolution, IEEE Transactions on Evolutionary Computation. 3(1) (1999) 22-34.

[27] R. K. Shrivastava, Differential Evolution Technique for Determining Shortest Distance to Voltage Collapse, International Journal of Engineering Trends and Technology (IJETT). 53(2) (2017) 80-88.

[28] D. G. Kurup at. al, Synthesis of Uniform Amplitude Unequally Spaced Antenna Arrays Using the Differential Evolution Algorithm, IEEE Transactions on Antennas and Propagation. 51(9) (2003) 2210-15.

[29] S. Cheng and C. Hwang, Optimal Approximation of Linear Systems by a Differential Evolution Algorithms, IEEE Transactions on Systems, Man Cybernetics-Part A: Systems and Humans. 31(6) (2003) 698-706.

[30] G. Antonini, SPICE Equivalent Circuits of Frequency-Domain Responses, IEEE Transactions on Electromagnetic Compatibility. 45(3) (2003) 502-12.